Raman Scattering Investigations of the Stable and Metastable Phases of Cyanoadamantane Glassy Crystal

Thomas Denicourt, Alain Hédoux,* Yannick Guinet, Jean-François Willart, and Marc Descamps

Laboratoire de Dynamique et Structure des Matériaux Moléculaires, UMR CNRS 8024, UFR de Physique, Bât. P5, Université des Sciences et Technologie de Lille, 59655 Villeneuve d'Ascq Cédex, France

Received: March 3, 2003; In Final Form: May 26, 2003

We report Raman investigations on stable and metastable phases of cyanoadamantane plastic crystal, which gives an orientational glassy state upon a deep undercooling below 175 K. The isothermal transformation of the metastable quenched plastic phase is systematically analyzed for quenches in the 180−250 K temperature range. Two different kinds of ordering process have been evidenced, depending on the depth of the quench. For shallow quenches (above 200 K) the ordering process is characterized by sigmoidal growth curves corresponding to the nucleation and growth of the ultimately stable state. For deep quenches (below 200 K), atypical kinetics laws are observed. In this case the system escapes from its metstable disordered state preferentially via the transient development of domains whose structure slightly differs from that observed in the ultimately stable phase, in agreement with Ostwald's rule of stages. The development of this local structure, after quenches at temperatures approaching T_g, is considered to be responsible for the extension of the lifetime of the metastability of the plastic phase and then could be at the origin of the glass formation.

Introduction

An especially challenging problem in the field of the physics of disordered materials is the understanding of the glass transition with the connected intense slowing down of molecular dynamics when approaching the glassy state.[1−4] Consequently, many experimental investigations have focused on the relaxation dynamics and the origin of the supercooled liquid state in molecular glass-forming liquids.[1−5]

Underlying the Vogel−Tamman−Fulcher (VTF) temperature behavior of supercooled liquids is the microscopic description of cooperative mechanisms that are recognized to develop in the metastable liquid states.[6−8] The existence of cooperatively rearranging regions (CRR's) is assumed in the model of Adam and Gibbs,[6] in which these domains are considered as dynamical entities. The growth of the CRR's, i.e., the increased cooperativity, is reflected in a loss of configurational entropy, which the Adam−Gibbs theory relates to an increase in the molecular relaxation time on approaching T_g, like more or less strong activation energy at T_g, which divides fragile liquids from strong liquids.[9] A fundamental question is to determine if the development of the cooperativity is associated with the concomitant development of some short-range order (SRO)[10,11] in the undercooled liquid. However, no experimental information about the structural signature of these dynamical domains has been yet detected in liquids, presumably because of the extreme difficulty in obtaining detailed structural information concerning the SRO in noncrystalline solids. Glassy crystals,[12,13] which are obtained by undercooling the rotator phase (plastic phase) of some molecular crystals, potentially offer an excellent opportunity to answer this question. In that case the freezing only involves the orientational degrees of freedom, on a lattice defined by the average center of mass of the rotating molecules. For undercooling of the plastic phase below an "orientational glass temperature", it is usually considered that the system is in a "glasslike" orientationally disordered state.[14] The persisting underlying crystalline structure makes these systems very promising to search for the structural origin of the frustration mechanism that leads to the glass.[13]

In this context, there is a considerable advantage to analyze supercooled plastic crystals with regard to supercooled liquids, where structural information cannot be detected in the broad radial function distribution or in the broad low-frequency vibrational band, respectively, from X-ray diffraction and Raman spectroscopy investigations. Moreover, in plastic crystals the frozen disorder can be easily characterized, since only the orientational degrees of freedom are involved in the process.

Cyanoadamantane (CNa) has been found to be a prototype of glassy crystals that has been extensively studied these last years.[15−20] At room temperature CNa is in the equilibrium state of a rotationally disordered cubic R-phase. The molecular dipoles can flip randomly along the six orientations defined by the 4-fold axis of the cubic cell ($Fm3m$).[21] This rotator phase is stable down to 283 K, where CNa crystallizes in an orientationally ordered monoclinic ($C2/m$) [22] "m-phase" (Figure 1). By rapid cooling, the ordering phase transition can be easily avoided, and after a quench far below 283 K,[23] DSC (differential scanning calorimetry) scans exhibit the Cp jump signature of conventional glasses at $T_g = 175$ K.[24] From dielectric experiments,[16] the relaxation time of dipolar flipping motion is determined to be close to 100 s near T_g, indicating that it is this very motion that gets frozen at T_g. Moreover, CNa has the advantage over other glassy crystals of providing single crystals of very high quality that can be deeply quenched without any damage.[13] Such properties have given researchers the opportunity to perform extensive X-ray diffraction experiments on quenched single crystals that have revealed the development of an antiferroelectric SRO[13,17,25] during the undercooling of the plastic phase. These SRO fluctuations were determined as being responsible for the decrease of configurational entropy

10.1021/jp0345405 CCC: $25.00
Published on Web 07/19/2003

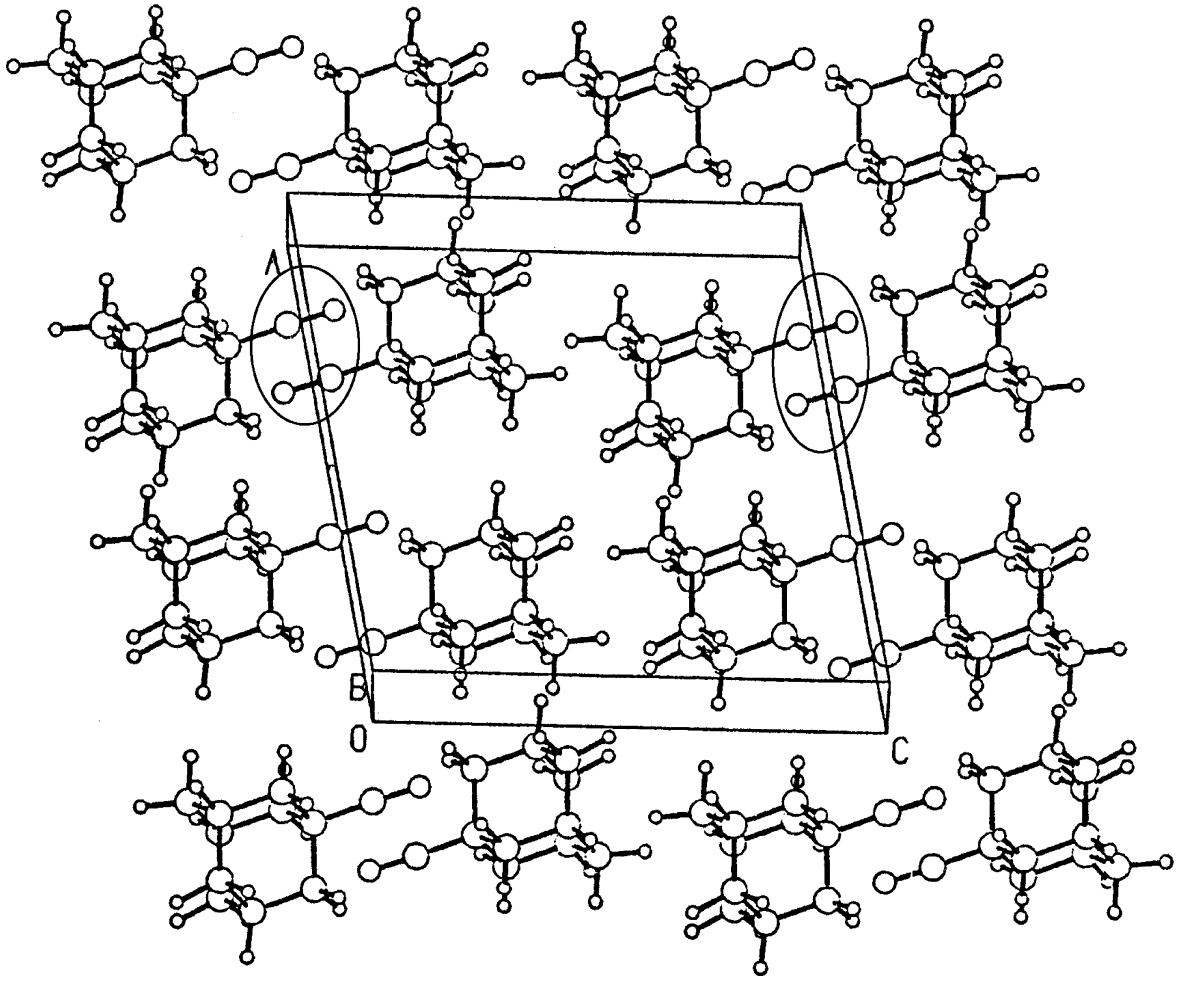

Figure 1. Representation of molecular arrangements in the m-phase from ref 22. Ellipses outline the hindrance in the bending vibration of C−C≡N protuberance in the (*a*, *c*) plane.

when approaching T_g and were identified as the structural signature of the CRR.[23,26] This description of the cooperative regions in CNa is quite different from the picture of independent zones emerging from that of Adam and Gibbs.[6] However, the destructive nature of the transformation toward the stable phase prevents detailed investigations of the subsequent long-range ordering by which the metastability is broken. Taking into account that the metastable states could develop on short time scales, time-resolved investigations on powder samples are needed to get additional information on the possible re-equilibration of the antiferroelectric short-range order after the quench.

During a sub-T_g aging, X-ray diffraction experiments[13,17,21,25] have revealed the development of a metastable state, through the detection of diffuse scattering intensity, prior to the ultimately stable monoclinic phase. This transient metastable state is characterized by spots at the forbidden points of the reciprocal lattice of the face-centered-cubic lattice (X boundary points of the Brillouin zone), which is indicative of an antiferroelectric order of molecules along one of the 4-fold cubic axes. This antiferroelectric transient structure is thus different from the antiferroelectric order of molecular dipoles along one of the cube diagonal's directions that ultimately develops in the low-temperature monoclinic phase.[22]

In this paper we report Raman investigations during the isothermal aging of quenched disordered states of CNa between 170 and 250 K. The ability of Raman spectroscopy to probe structural modifications on a short length scale with a high temporal resolution provides information on the development of the antiferroelectric local order during the isothermal ordering process.

Experimental Section

The powder sample was introduced in a Lindemann glass capillary (diameter 1.0 mm). Low-temperature Raman experiments were performed using an Oxford cryostream low-temperature device. The rotator phase of CNa was quenched from room temperature down to the aging temperature T_a by shifting the sample in the well-regulated nitrogen flux. The Raman spectra were excited with a 514.5 line of a mixed argon−krypton coherent laser. The backscattering light was analyzed in a XY Dilor spectrometer equipped with a N_2-cooled CCD system. The isothermal transformations of CNa can be carefully analyzed by taking spectra every minute for rapid isothermal transformations (in the 200−240 K temperature range). The time acquisition was 50 s to obtain a well-defined spectrum covering the 5−600 cm^{-1} frequency range. Parameters of Raman bands (frequency, width, intensity) were determined by a fitting procedure based on the residual method using damped oscillators.

Results

1. The Raman Spectrum of CNa in the Disordered and Ordered Phases. The Raman spectra of both the disordered and ordered phases are plotted on Figure 2 in the investigated frequency range (5−600 cm^{-1}); they can be classically divided in two parts.

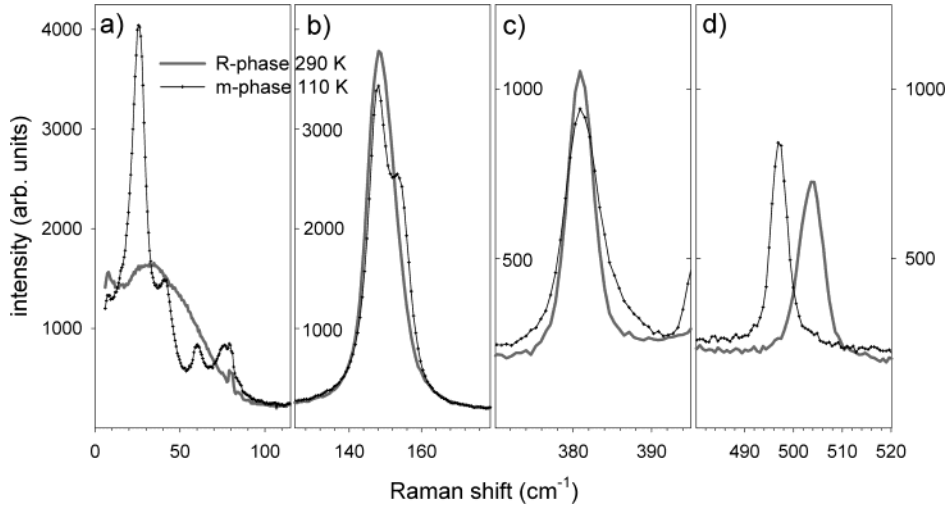

Figure 2. The Raman spectra of the stable R- and m-phases of CNa in the (a) low-frequency region, (b) bending mode region, (c) [370, 395 cm^{-1}] range, (d) [480, 520 cm^{-1}] range.

(i) The lattice mode region is lying in the low-frequency range below 120 cm^{-1} at room temperature. In the plastic phase the low-frequency Raman intensity is observed (Figure 2a) to be dominated by a broad feature, i.e., a phonon density of states as expected for a highly disordered system. In this context the Raman intensity can be described as usual[27]:

$$I_{\text{Raman}}^{\text{obs}} \propto \left[1 - \exp\left(\frac{-h\omega}{kT}\right)\right]^{-1} \frac{C(\omega)\, g(\omega)}{\omega} \qquad (1)$$

where $C(\omega)$ is the phonon−photon coupling function and $g(\omega)$ the vibrational density of states.

In the low-frequency Raman spectrum of the ordered monoclinic phase (Figure 1a) six modes are detected at low temperature (110 K) as expected from symmetry considerations:

$$\Gamma_{\text{ext}} = 3A_g + 3B_g\,(\text{Raman active}) + 2A_u + 1B_u\,(\text{IR active}) \qquad (2)$$

In Figure 2a, the broad low-frequency band in the Raman spectrum of the rotator phase can be reasonably identified as the envelope of the phonon peaks of the ordered phase.

(ii) The isolated CNa molecule ($C_{10}H_{15}CN$) has C_{3v} symmetry and possesses 75 internal modes in the plastic phase ($Fm3m$, $Z = 4$) as for the free molecule:

$$\Gamma_{\text{int}} = 17A_1 + 8A_2 + 25E \qquad (3)$$

In the investigated internal-mode region lying from 120 cm^{-1} up to 600 cm^{-1}, three spectral windows corresponding to parts b, c, and d in Figure 2 were carefully analyzed:

(1) In the 120−180 cm^{-1} region (Figure 2b) the internal E-mode, corresponding to the C−C≡N distortion with respect to the molecular axis (the so-called bending mode), is observed near 150 cm^{-1} at room temperature. This mode is very interesting, because it is the only Raman active mode in the 120−180 cm^{-1} range and then was found to be a very sensitive probe of the local ordering,[28] as explained in the following. Because of the lowering of the symmetry passing through the disorder−order phase transition, the E modes split into the (A_g, B_g) doublet, as observed in Figure 2b. The symmetry assignment of these two bands was made in a previous analysis[28] performed on single crystals. The low-frequency component (B_g mode) is an in-phase and out-plane bending, and the high-frequency component (A_g mode) corresponds to an in-phase and in-plane bending. Figure 3 clearly reveals a strong temperature dependence of the A_g mode with regard to the B_g mode. This special temperature behavior for an internal mode can be understood from the consideration that the vibration in the (a, c) plane is very sensitive to interactions between two CN of two neighboring molecules, as can be observed in Figure 1. From symmetry arguments,[28] only one E-symmetry band is expected in the R-phase. Consequently, the asymmetric line shape of the bending mode in the disordered state was assigned to the existence of an antiferroelectric SRO, reminiscent of the long-range order (LRO) of the ultimately stable phase. After quench below 283 K, the line shape of the bending band remains asymmetric and a very slight frequency shift of the "A_g" component is detected by the fitting procedure (Figure 3). This observation demonstrates that the SRO is —at least—preserved during the quench in the temperature range where the plastic phase is metastable. The difference between the frequencies of the A_g mode in the ordered stable phase and undercooled disordered state indicates that this SRO is not a precursor of the ultimately stable state.

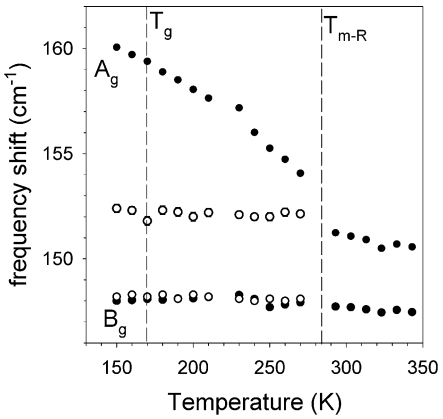

Figure 3. Temperature dependence of the components of the bending band in the R- and m-phases. Open circles correspond to the frequencies of the bending modes recorded in the metastable R-phase just after the quench. Full circles to the frequencies of the same bands in the stable ordered m-phase and in the disordered R-phase.

(2) The Raman bands observed in the 300−600 cm^{-1} frequency range (Figure 2c,d) can be assigned to A_1 species, since they do not split below 283 K. In this spectral range two Raman bands exhibit different behaviors passing through the

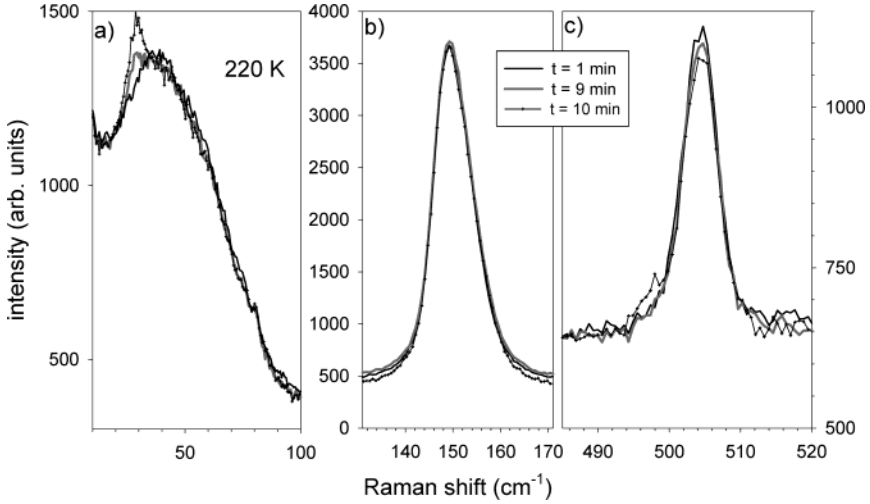

Figure 4. The time dependence of the Raman spectrum in the earliest stages of the ordering process after a quench of the R-phase down to 220 K (a) in the low-frequency range, (b) in the bending mode region, (c) in the 485−520 cm^{-1} frequency range.

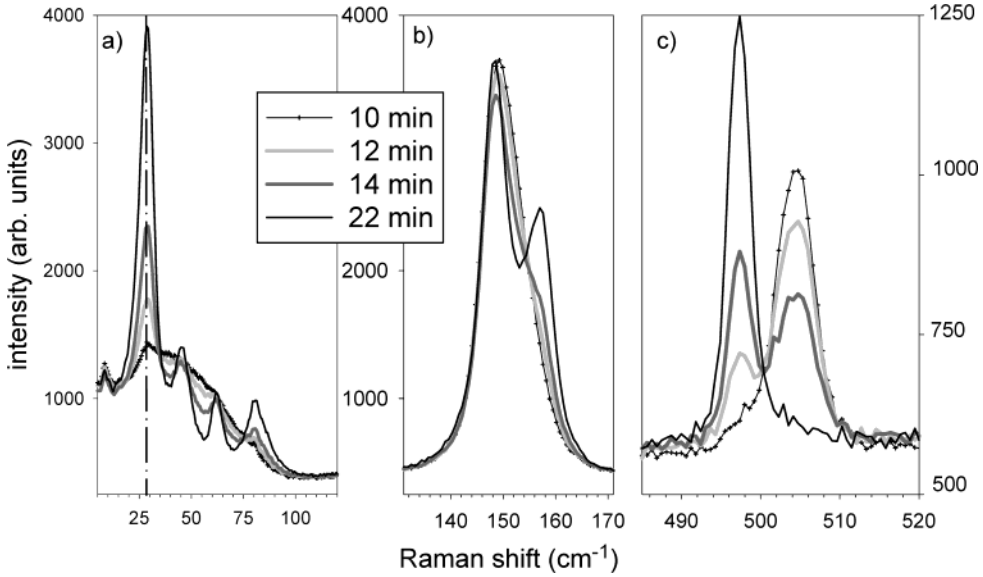

Figure 5. The time dependence of the Raman spectrum 10 min after the quench at 220 K.

phase transition, as can be observed in figure 2c,d. The 382 cm^{-1} Raman band exhibits no frequency shift and no significant change of intensity through the ordering phase transition, while the 505 cm^{-1} band shifts from 505 to 496 cm^{-1}. Taking into account the first-order character of the phase transition, a coexistence of the disordered and ordered phases is expected during isothermal transformation and, thus, the coexistence of the two A_1 and A_g Raman modes also. Consequently, the analysis of this spectral window should provide information about the kinetics of an isothermal transformation. Since the 382 cm^{-1} Raman band is temperature independent, the transformation rate toward the ordered state can conveniently be derived from the ratio I_{496}/I_{382}.

2. Kinetics of Ordering. (i) Ordering Process after Quenches in the Temperature Range [200, 250 K].

Raman investigations were carried out after quenches at T_a = 200, 210, 220, 240, and 250 K. Figure 4 shows a detailed analysis of the isothermal ordering process at 220 K.

The first stage of the time evolution (t < 10 min) of the low-frequency Raman intensity is reported in Figure 4a. It shows that the first trace of transformation appears clearly in the low-frequency range 9 min after the quench of the sample, through the emergence of a Raman band at 26 cm^{-1}. This band corresponds to the most intense phonon peak of the stable phase, and no other change is detected in the line shape of the low-frequency spectrum. At higher frequencies, no perceptible change can be detected on the line shape of the bending band (Figure 4b), while a very slight decrease of intensity of the 505 cm^{-1} Raman band is observed (Figure 4c). One minute later (t = 10 min) this intensity decrease is enhanced and accompanied by a tailing on the low-frequency side of the corresponding band (Figure 4c).

In the second stage (t > 12 min, Figure 5a), the line shape of the broad vibrational band is structuring while the low-frequency band around 26 cm^{-1} is growing. At t = 22 min the line shape of the low-frequency Raman spectrum corresponds rigorously to that of the ordered monoclinic phase, which indicates that the transformation toward the ultimately stable phase is completed. The emergence of the 26 cm^{-1} band can be considered as the most sensitive Raman signature of the ordering process toward the ultimately stable phase. At higher frequencies (Figure 5b), the asymmetric character of the bending band is enhanced, leading to the splitting of the E mode into the (A_g, B_g) Davydov doublet. The time dependence of the frequencies of the A_g and B_g modes is determined by fitting the Raman spectrum in the 135−175 cm^{-1} region with two

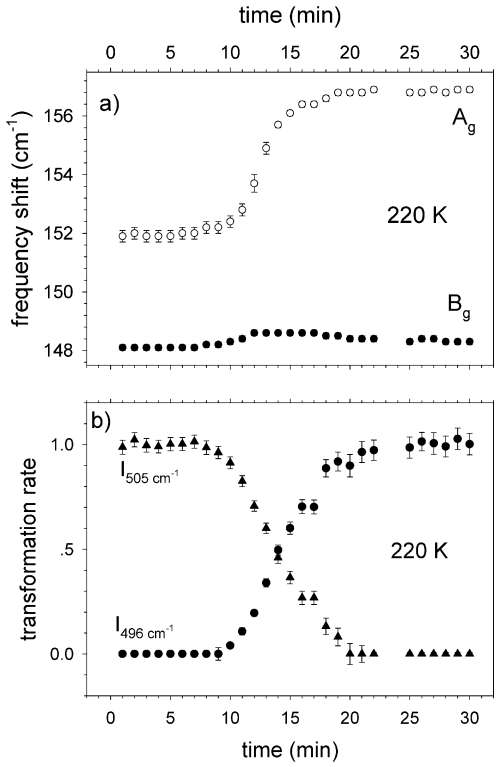

Figure 6. The time dependence of the Raman signatures of the isothermal ordering process at 220 K. (a) The frequency shift of the bending modes. (b) The concomitant decrease and increase of the intensities of the 505 (triangles) and 496 cm^{-1} (circles) bands renormalized to the intensity of the 382 cm^{-1} band. The circles correspond to the transformation rate into the ordered state.

damped oscillators and plotted in Figure 6a. The asymmetric line shape of the bending band in the metastable rotator phase reveals that the SRO is preserved by quenching the sample, and the time dependence of the high-frequency component is indicative of the growth of the LRO of the stable ordered phase. The analysis of the spectral window around 500 cm^{-1} is performed from a fitting procedure of the 496 and 505 cm^{-1} bands. The transformation rates calculated from the time dependence of the intensity (normalized to unity) of these Raman bands characteristic of the rotator phase (505 cm^{-1}) and the ordered phase (496 cm^{-1}) are reported on Figure 6b. This figure demonstrates that the growth of the 496 cm^{-1} band corresponds rigorously to the concomitant intensity decrease of the 505 cm^{-1} band, as can be observed in Figure 5c. In this context, the time dependence of the intensity of the 496 cm^{-1} band can be reasonably considered as the growth curve of the m-phase. This growth curve has a sigmoidal shape nearly symmetrical with respect to the half-completion time ($t_{1/2} = 14$ min at $T = 220$ K). Such a sigmoidal shape is expected for the time evolution of the transformed fraction, which describes how the system escapes from metastability to reach the most stable state.

(ii) Ordering Process after Quenches below 190 K. The time dependence of the low-frequency Raman spectrum during the isothermal aging at $T_a = 190$ K is plotted in Figure 7. At the earliest stages of the transformation (Figure 7a), a very subtle change in the line shape of the low-frequency vibrational band can be detected a few minutes after the quench down to 190 K. At $t = 9$ min, one can recognize the emergence of the low-frequency band near 26 cm^{-1} considered as the Raman signature of the ordering process, accompanied at higher frequencies (around 150 and 505 cm^{-1}) by Raman features similar to those previously described at 220 K. The time dependence of these Raman features, plotted in Figure 8, resembles that previously observed at 220 K. Figure 7 shows that the scenario of the transformation is similar to that described at 220 K, except for the change in the line shape of the broad low-frequency librational band at the earliest stage of the transformation.

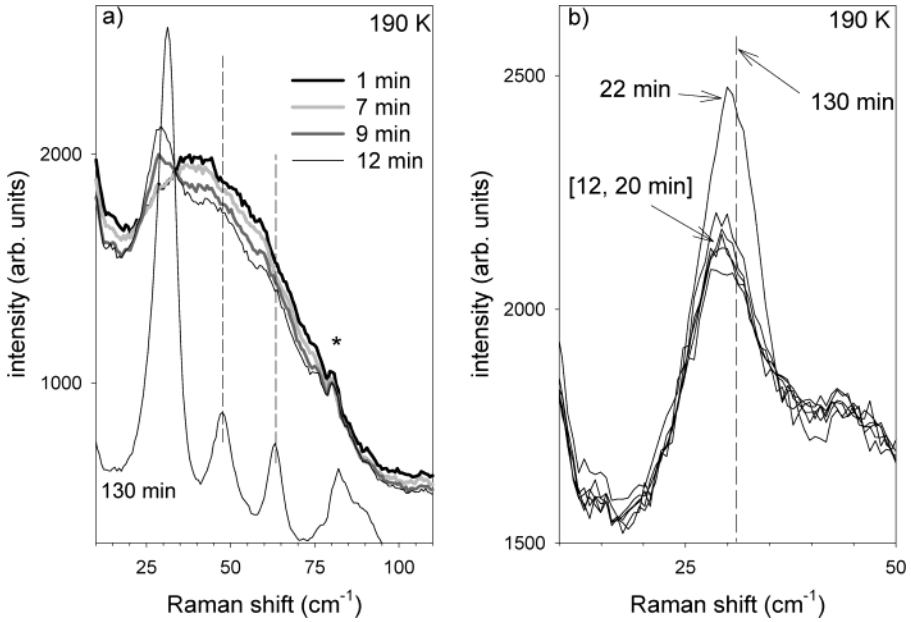

Figure 7. The time dependence of the low-frequency Raman spectrum after a quench down to 190 K. (a) The Raman spectrum in the earliest stages of the ordering process is compared to that of the ordered m-phase. A clear frequency shift of the initial shoulder (near 26 cm^{-1}) is observed over the course of the transformation toward the m-phase. Moreover, dashed lines reveal the discrepancies between initial structuring features (at $t = 1$ min) and the phonon peaks of the m-phase ($t = 130$ min) indicative of a change in the local order during the isothermal transformation. (b) A detailed investigation in the 10−50 cm^{-1} range reveals the existence of a transient stage in the course of the ordering process. This stage corresponds to the distinctive intensity and frequency of the low-frequency band. This frequency is observed to be different than that of the corresponding phonon peak in the m-phase localized by the dashed line. This demonstrates that the medium-range order in the transient state is different from that of the m-phase.

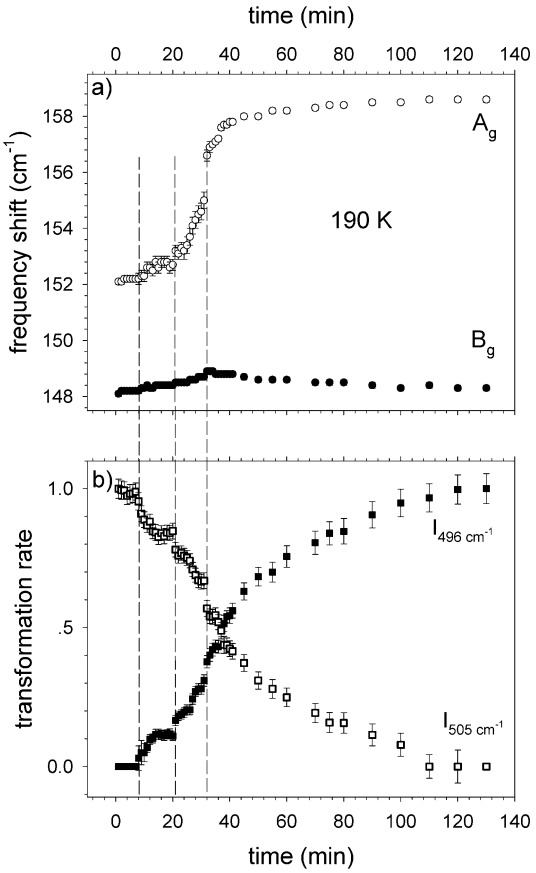

Figure 8. The time dependence of the Raman signatures of the ordering process at 190 K. (a) The frequency shift of bending modes. (b) The concomitant increase and decrease of the intensities of the 496 and 505 cm^{-1} Raman bands. The dashed lines point out a similar time dependence on different types of information. These coincidences reflect that the transformed matter (corresponding to a volume determined from a) in the ordering process is characterized by a distinct local order (corresponding to the frequency of the "A_g" mode in b).

However, the increase of the intensity of the emerging 26 cm^{-1} band is stopped during about 10 min in the range [12, 20 min] (Figure 7b). It is worth noticing that this observation corresponds to a stage in the time dependence of Raman features observed during the transformation, i.e., the frequency shift of the high-frequency component of the bending band (Figure 8a) and the intensities of the 496 and 505 cm^{-1} bands (Figure 8b). These irregularities suggest the existence of an intermediate state in the ordering process. Some structuration emerges from the line shape of the low-frequency spectrum taken at the stage 12−20 min (Figure 7a), roughly corresponding to the envelop of phonons of the ultimately ordered phase. It can be noticed in Figure 7a that the structurations emerging from the low-frequency Raman spectrum at t =12 min are shifted with respect to the phonons of the ordered m-phase (localized by dashed lines). At this stage, the Raman spectrum of CNa mirrors the existence of nuclei whose LRO is different from that of the ordered m-phase.

After this stage, the emergence of the low-frequency band is accompanied by a slight frequency shift (Figure 7a,b). The low-frequency spectrum continuously sharpens versus time, accompanied by a significant frequency shift of Raman bands toward the phonon peaks of the low-temperature phase. The confrontation of Figure 8a,b reveals that the time dependence of the frequency of the "A_g" bending mode and the time dependence of the Raman intensity of the 496 and 505 cm^{-1} bands are fully similar and exhibit the same irregularities. This indicates that the different stages of the ordering process corresponds to the production of different transient structural organizations.

Discussion

From these results, two different kinds of ordering processes are detected, depending on the depth of quench.

For a shallow quench (above T_a = 200 K), the ordering process can be analyzed as follows. At the earliest stages of the isothermal aging an initial plateau is observed. Its length corresponds to the life-time of metastability of the R-phase. After this stage, the observation of a low-frequency shoulder emerging near 26 cm^{-1} indicates that the system escapes from metastability. This occurs through nucleation of clusters in which one can recognized the LRO of the ultimately stable phase, since the low-frequency shoulder rigorously corresponds to the most intense phonon peak of the ordered phase. The intensity increase of the 496 cm^{-1} Raman band is accompanied by the structuration of the broad low-frequency vibrational band, the development of the shoulder near 26 cm^{-1}, and the splitting of the bending band. Consequently, the intensity of the 496 cm^{-1} band normalized to unity is clearly connected to the development of the LRO and then is considered as the transformation rate into the stable phase. The growth curves determined from the time dependence of the 496 cm^{-1} Raman band for isothermal aging performed in the [200, 250 K] temperature range, have been fitted using an Avrami-like function according to

$$I_{norm}(496\ cm^{-1}) = \frac{I(496cm^{-1})}{I(382cm^{-1})} \propto (1 - \exp(-[t/t_{1/2}]^n)) \quad (4)$$

The parameters ($t_{1/2}$, n) obtained from the fitting procedure using eq 4 for all transformations between 200 and 250 K are reported in Table 1, and the growth curves rescaled to $t_{1/2}$ are plotted in Figure 9a. The latter and Table 1 show that the growth curves exhibit roughly the same scaling law that is satisfactorily described by eq 4. Typical sigmoidal shapes strongly suggest that the ordering process (in this temperature range) is controlled by a nucleation and growth mechanism. A significant deviation of the exponent value (n = 11) for the isothermal transformation at 250 K, certainly inherent to the length of the initial plateau, can be noticed. In this temperature range the time of transformation is controlled by the thermodynamic parameters (driving force and nucleation barrier) responsible for the long-living metastability of the R-phase.

For a deep quench (below 200 K) the growth curves were determined during isothermal transformation at 190 and 180 K (just above T_g = 175 K) and plotted in Figure 9b. Both curves exhibit significant deviations from the sigmoidal shape observed for isothermal aging above 200 K. They also exhibit an initial plateau indicative of the lifetime of the metastable R-phase.

The appearance of the low-frequency shoulder near 26 cm^{-1}, slightly shifted with regard to the frequency of the most intense phonon peak of the stable phase, indicates the nucleation of a LRO slightly different from that of the stable phase. The antiferroelectric SRO detected at room temperature (in the R-phase) by X-ray diffraction experiments[23] was observed to develop during a quench below 200 K[23] and then was considered as a precursor of this LRO. Consequently, this LRO is likely to be responsible for the intermediate stages observed after 10 min at 190 K and for some other irregularities detected in the growth curves (Figure 9b). As a consequence, the growth curves

TABLE 1: Parameters of the Avrami Law Defined in Eq 5 for Isothermal Transformations in the 200−250 K Temperature Range for Deep Quenches (below 200 K)[a]

T (K)	180	190	200	210	220	240	250
n			6.1 ± 0.5	5.8 ± 0.5	4.6 ± 0.4	4.7 ± 0.4	11.0 ± 0.7
$t_{1/2}$ (min)	~ 320[a]	~ 40[a]	39.0 ± 0.2	17.0 ± 0.1	15.7 ± 0.2	33.0 ± 0.2	217.1 ± 0.6

[a] Times at half-transformation are graphically determined.

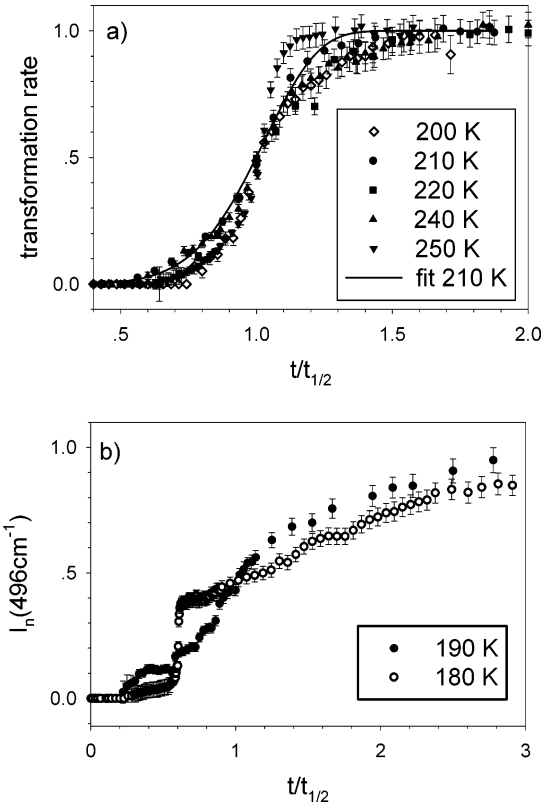

Figure 9. Scaled growth curves corresponding to the normalized intensity during isothermal transformations after a quench from room temperature down to T_a: (a) in the 200−250 K range and (b) below 200 K.

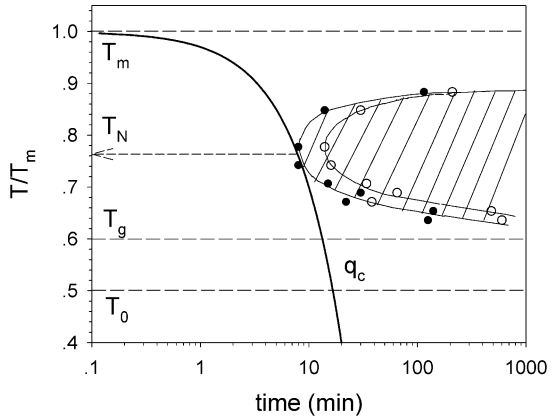

Figure 10. Time−temperature−transformation (TTT) diagram. Open circles correspond to the half-transformation rate, while full circles correspond to the detection of the first traces of transformation. $T_m = 283$ K, $T_g = 170$ K, and T_0 (corresponding to the temperature where the viscosity is infinite) is reported as $T_m/2$ from ref 31. T_N is determined from the diagram as the "nose" temperature or from ref 31. q_c is the minimal cooling rate for which the formation of the glass is still possible.

correspond to atypical kinetic laws that are clearly different from those obtained after a quench above 200 K and described by a sigmoidal shape. These atypical kinetic laws indicate a change in the ordering mechanism below 200 K. The observation of stages and other irregularities in the growth curves suggest the existence of intermediate states and short-living intermediate metastable modifications. These transient metastable states would be necessary for the achievement of the complete ordering in the low-temperature range, i.e., when the development of the SRO hinders the nucleation of the stable monoclinic phase.

All the features observed during the isothermal ordering process below 200 K and described above are compatible with Ostwald's rule of stages.[29] From Ostwald's experience, a metastable state does not directly transform into the stable state but prefers to reach intermediate stages. According to Ostwald's rule of stages, the possibility of transformations between two or more fluxes of different new phase clusters could be responsible for the atypical kinetic laws determined for isothermal ordering process below 200 K. It is reasonable to consider that this mechanism is preferentially observed in the low-temperature region ($T < 200$ K), where the development of the SRO in the metastable R-phase, which is not a precursor of the m-phase, makes the nucleation and growth of the latter more difficult. The deeper the quench, the more developed these SRO fluctuations and the longer ordering kinetics. In this context, it can be considered that the development of SRO fluctuations increasingly makes difficult the nucleation of the ordered m-phase as the quench temperature approaches T_g. This behavior results in an increase of the life-time of the disordered metastable R-phase in regard to the most stable m-phase. It thus promotes the formation of the glassy state by making easier the undercooling of the R-phase.

The ability of our Raman spectrometer to detect the first traces of crystallization through subtle changes in the shape of the broad low-frequency vibrational band has led to the determination of the kinetic criterion for vitrification.[30] From the latter, any substance can be vitrified by a fast enough cooling. The minimal cooling rate required for vitrification can be estimated from the plot of the T(time)−T(temperature)−T(transformation) diagram. This diagram is plotted in coordinates (T/T_m) versus log t, as proposed by Gutzov,[31] where T_m corresponds to the melting temperature for a glass-forming liquid. The temperature T_0, where the viscosity is expected to diverge for conventional glasses, is empirically considered as $T_m/2$. TTT-curves corresponding to the half-transformation rate ($\tau_{1/2}$) and the lower limit (τ_c) of detection of crystallization are reported in Figure 10. The latter displays a nonmonotonic temperature dependence of the time required to obtain a given volume fraction of ordered phase, as expected from TTT-diagrams of glass-forming liquids.[8,31] This behavior is usually considered to reflect the competition between the thermodynamic driving force for nucleation and viscous effects. In the case of CNa, the extent of undercooling of the R-phase is connected to the development of the antiferroelectric SRO existing from room temperature, which is recognized as the structural signature of the CRR.[23,26]

From Figure 10, a minimal cooling rate, q_c, can be determined. Considering constant cooling rates, q-curves, the linear T versus t dependencies are transformed into curves plotted in the TTT diagram (Figure 10), where the q_c-curve is tangent to the $t(\tau_c)$-curve at the "nose" temperature, T_N. T_N can be

approximately determined by[31]

$$T_N \approx \frac{1}{2}(T_m + T_0) \quad (5)$$

From this relation we get $T_N \approx 212$ K, while from experimental data reported on the TTT-diagram T_N corresponds approximately to 215 K. From eq 3, q_c can be defined as

$$q_c = \frac{T_N}{t_N(\tau_c)} \cong \frac{1}{2}\left(\frac{T_m + T_0}{t_N(\tau_c)}\right) \quad (6)$$

The estimation of $t_N(\tau_c) \approx 8$ min (at which T_N is reached) from the TTT-diagram leads to the determination of the minimal cooling rate, $q_c \approx 30$ K/min, required to obtain the glassy state of CNa. The uncertainty on the determination of q_c is highly dependent on the method of detection of the first traces of crystallization. The lowest value of detectable crystallization is not quantifiable, since the first traces of crystallization are detected from the analysis of the broad low-frequency vibrational band, while no intensity can be measured at 496 cm^{-1}. However, this value can be estimated near 10^{-3} for a structural probe, while a degree of crystallization of 10^{-6} can be determined from optical microscopic methods of investigation, in the most favorable cases.

Conclusion

Raman investigations in the different states of CNa provide important information about both the ordering process by which the metastable R-phase transforms toward the ultimately stable m-phase and also in the route of the plastic crystal toward the glassy crystal state.

These Raman data confirm the existence of an antiferroelectric SRO in the R-phase at room temperature through the asymmetric shape of the bending band. The development of the antiferroelectric SRO, observed (by X-ray diffraction experiments[23]) during the life of the metastable R-phase if the plastic phase is quenched in a far-from-equilibrium situation (below 200 K), can be considered as a precursor of the observation of intermeditate states described by the shape of the low-frequency Raman spectrum by nanodomains in the matrix of the R-phase. The LRO characterizing these domains would be slightly different from that of the stable low-temperature phase.

As a consequence, the metastable R-phase isothermally transformed into the m-phase following atypical kinetic laws, connected to the emergence of intermediate metastable states, predicted by Ostwald's rule of stages. The present investigations reveal that the SRO in the metastable R-phase is responsible for a frustration between the development of the SRO fluctuations and that of the ordered m-phase. This frustration strongly increases the life-time of metastability of the quenched plastic phase and, by the way, develops its undercooling properties and thus its glass-forming ability.

This study shows the influence of microscopic rearrangements in the metastable plastic phase on the ordering mechanism of CNa. However, their structural description is quite different from that of Adam and Gibbs in terms of dynamical entities (CRR), since they were determined as corresponding to fluctuations of the antiferroelectric local order.[16,25]

References and Notes

(1) Anderson, P. W. *Science* **1995**, *267*, 1615.
(2) Ediger, M. D.; Angell, C. A.; Nagel, S. R. *J. Phys. Chem.* **1996**, *100*, 13200.
(3) Ngai, K. L. *J. Non-Cryst. Solids* **2000**, *275*, 7.
(4) Angell, C. A.; Ngai, K. L.; McKenna, G. B.; McMillan, P. F.; Martin, S. W. *J. Appl. Phys.* **2000**, *88*, 3113.
(5) Lunkenheimer, P.; Schneider, U.; Brand, R.; Loidl, A. *Contemp. Phys.* **2000**, *41*, 15.
(6) Adam, G.; Gibbs, J. H. *J. Chem. Phys.* **1965**, *43*, 139.
(7) Jackle, J. *Rep. Progr. Phys.* **1986**, *49* (2), 171.
(8) Debenedetti, P. G. *Metastable Liquids—Concepts and Principles*; Princeton University Press: Princeton, NJ, 1996.
(9) Angell, C. A. *J. Phys. Chem.* **1988**, *49*, 863.
(10) Ernst, R. M.; Nagel, S. R.; Grest, G. S. *Phys. Rev. B Condens. Matter* **1991**, *43*, 8070.
(11) Leheny, R. L.; Menon, N.; Nagel, S. R.; Price, D. L.; Suzuya, K.; Thiyagarajan, P. *J. Chem. Phys.* **1996**, *105*, 7783.
(12) Suga, H.; Seki, S. *J. Non-Cryst. Solids* **1974**, *16*, 171.
(13) Descamps, M.; Willart, J. F.; Odou, G.; Eichhorn, K. *J. Phys. 1* **1992**, *2*, 813.
(14) Brand, R.; Lunkenheimer, P.; Loidl, A. *J. Chem. Phys.* **2002**, *116*, 10386.
(15) Amoureux, J. P.; Castelain, M.; Bee, M.; Arnaud, B.; Shouteenten, M. L. *Mol. Phys.* **1981**, *42*, 119.
(16) Amoureux, J. P.; Castelain, M.; Benadda, M. D.; Bee, M.; Sauvajol, J. L. *J. Phys.* **1983**, *44*, 513.
(17) Descamps, M.; Caucheteux, C. *J. Phys. C Solid-State Phys.* **1987**, *20*, 5073.
(18) Descamps, M.; Caucheteux, C.; Odou, G. *J. Phys. (Colloque)* **1985**, *46*, 329.
(19) Descamps, M.; Willart, J. F.; Kuchta, B.; Affouard, F. *J. Non-Cryst. Solids* **1998**, *235*, 559.
(20) Rolland, J. P.; Sauvajol, J. L. *J. Phys. C* **1986**, *19*, 3475.
(21) Willart, J. F.; Descamps, M.; Benzakour, N. *J. Chem. Phys.* **1996**, *104*, 2508.
(22) Foulon, M.; Amoureux, J. P.; Sauvajol, J. L.; Cavrot, J. P.; Muller, M. *J. Phys. C Solid-State Phys.* **1984**, *17*, 4213.
(23) Willart, J. F.; Descamps, M.; van Miltenburg, J. C. *J. Chem. Phys.* **2000**, *112*, 10992.
(24) Foulon, M.; Amoureux, J. P.; Sauvajol, J. L.; Lefebvre, J.; Descamps, M. *J. Phys. C Solid-State Phys.* **1983**, *16*, L265.
(25) Willart, J. F.; Descamps, M. *Progr. Theoret. Phys.* **1997**, *126*, 239.
(26) Affouard, F.; Willart, J.-F.; Descamps, M. *J. Non-Cryst. Solids* **2002**, *307−310*, 9.
(27) Shucker, R.; Gammon, R. W. *Phys. Rev. Lett.* **1970**, *25*, 222.
(28) Guinet, Y.; Sauvajol, J. L. *J. Phys. C Solid-State Phys.* **1988**, *21*, 3827.
(29) Ostwald, W. *Z. Phys.* **1897**, *22*, 286.
(30) Uhlmann, D. R. *J. Non-Cryst. Solids* **1972**, *7*, 337.
(31) Gutzow, I.; Schmelzer, J. *The Vitreous State: Thermodynamics, Structure, Rheology, and Crystallization*; Springer: Berlin, 1995.